Available online at www.sciencedirect.com
SCIENCE DIRECT®
Journal of Sound and Vibration 289 (2006) 726–744
JOURNAL OF SOUND AND VIBRATION
www.elsevier.com/locate/jsvi

Octo-strut vibration isolation platform and its application to whole spacecraft vibration isolation

L.K. Liu*, G.T. Zheng, W.H. Huang

Department of Space Engineering and Applied Mechanics, Harbin Institute of Technology, P.O. Box 137, Harbin Institute of Technology, Harbin 150001, PR China

Received 21 January 2004; received in revised form 25 January 2005; accepted 18 February 2005
Available online 3 June 2005

Abstract

Stewart platform is widely used for vibration isolation and precise pointing. As it is a statically determinate structure, if any strut has fault, a disaster could be unavoidable. In the present paper, an octo-strut passive vibration isolation platform with redundancy is introduced and applied to whole-spacecraft vibration isolation. This platform is modeled with the Newton–Euler method. To avoid such possibility that the spacecraft may interact with the fairing, an approach of stiffness design is proposed to reinforce the rotation stiffness of the platform. With the mathematical model, design parameters of the isolator that will affect the nature frequencies of the isolator-spacecraft system are studied. The transmissibility of the isolator topped with rigid and flexible spacecraft is also studied. Results of analytical and numerical studies show that the octo-strut platform is a reliable and effective approach to improving the dynamic environment of a spacecraft.
© 2005 Elsevier Ltd. All rights reserved.

1. Introduction

A number of researchers have investigated the use of Stewart platform (or hexapods) for vibration isolation and precise pointing. For space applications Stewart platforms have the inherent capability of providing articulation between subsystems as well as vibration isolation

*Corresponding author. Tel.: +86 451 86418029; fax: +86 451 86418873.
E-mail addresses: liulk@hit.edu.cn (L.K. Liu), gtzhengtu@yahoo.co.uk (G.T. Zheng), whhuang@hit.edu.cn (W.H. Huang).

0022-460X/$ - see front matter © 2005 Elsevier Ltd. All rights reserved.
doi:10.1016/j.jsv.2005.02.040

Nomenclature

$\{B\}$	reference frame rigidly attached to the base
$\mathbf{C}$	vector containing all Coriolis and centripetal terms
dof	degree of freedom
$\mathbf{F}_s$	generalized force acting on the payload-interface applied by the struts
$\mathbf{G}$	vector containing all gravity term
H_c	height of the satellite's centroid
${}^U\mathbf{I}$	inertia matrix of the payload in the universal inertial frame
$\mathbf{J}$	Jacobian matrix of the platform
${}^U\mathbf{M}$	mass/inertia matrix of payload in the universal inertial frame
N	number of struts, for the octo-strut platform, $N = 8$
$\{P\}$	reference frame rigidly attached to the payload-interface
${}^U\mathbf{P}_{B_{\mathrm{ORG}}}$	position of the origin of frame $\{B\}$ in $\{U\}$
R_l	radius of the low ring
R_u	radius of the up ring
${}^U_B\mathbf{R}$	transformation matrix from $\{B\}$ to $\{U\}$
$\{U\}$	universal inertial reference frame
f_{pi}	axial force acting on the ith strut applied by the payload-interface
h	platform height
k	mount stiffness of a single strut
k_c	coupling stiffness of two struts
l_i	instantaneous length of the ith strut
l_{ri}	relaxed length of the ith strut
m_{si}	moving mass of the ith strut
$\mathbf{p}_i$	position of the point connecting the PI and the ith strut
PAF	payload attaching fitting
PIP	rigid bode composed of the payload-interface and the payload
$\mathbf{q}_i$	position of the point connecting the base and the ith strut
m	mass of the payload
WSVI	whole-spacecraft vibration isolation
$\mathbf{x}_B$	position and attitude of $\{B\}$
$\mathbf{x}_P$	position and attitude of $\{P\}$
$\boldsymbol{\omega}_P$	angular velocity of $\{P\}$
$\boldsymbol{\omega}_B$	angular velocity of $\{B\}$
θ	included angle of a pair of struts

with the same mechanical system. Consequently system complexity and weight can be significantly reduced. Geng and Haynes [1] developed an active vibration isolation system using a Stewart platform of cubic configuration along with robust adaptive filter algorithms for active vibration control. Spanos et al. [2] conducted analytical and experimental research with a six-axis actively controlled vibration isolator that consists of six active struts, each of which includes an electromagnetic voice coil actuator in parallel with a soft spring. Six decoupled analog controllers were used to close broad-band feedback loops around six force sensors. Through Newton–Euler approach, Dasgupta and Mruthyunjaya [3] derived closed-form dynamic equations for two widely used kinematic structures of Stewart platform, namely the six-UPS structure with universal joints at base-connection-points of struts and six-SPS structure with spherical joints at both ends of struts. The inertial effect of the strut rotation in a Stewart platform was studied by Ji [4]. McInroy and Hamann [5], McInroy [6,7] and McInroy et al. [8] developed a dynamic model of flexure jointed hexapods with base acceleration and derived the decoupling conditions for the need of active control.

However, the Stewart platform is a statically determinate structure, if any strut has fault, disaster could be unavoidable. In order to meet high requirement for reliability in space applications, it is desired that redundancy should be provided by adding more struts to the platform. In this paper, an octo-strut platform that has eight struts will be investigated. Although

this octo-strut platform might not be the best structure for all applications, in the application of Whole-Spacecraft Vibration Isolation (WSVI), under the constraint conditions of size and space, and importantly the requirement of isolating vibrations in a three-dimensional space, it provides the required included angle between the strut and the base for the strut to function in all directions, and in the meantime is able to provide sufficient redundancy for the purpose of safety and reliability.

The octo-strut platform will be applied to realize the WSVI, which can significantly improve the dynamic environment that a launch can provide to its payload. The idea of WSVI proposed here is to use this octo-strut platform to replace the existing Payload Attaching Fitting (PAF), which is used to provide an interface between the launch vehicle and the spacecraft, which traditionally is designed very stiff for restricting the relative motion between the spacecraft and the faring.

In space industries, two of the important challenges are the minimum structural mass of a spacecraft and the maximum market of a launch vehicle. A major factor, which determines whether these targets can be reached or not, is the dynamic environment that a launch vehicle can provide. The launch stage is the most severe dynamic environment that a spacecraft will experience during its mission life. To survive the launch stage, the structure of a spacecraft has to be strengthened by adding extra structural mass that will be useless in the operating orbit. This not only increases launch costs, but also reduces the mass margin that could be used for launching additional payload. As there are more and more launch service providers in the world, spacecraft owners now have more choices than ever before. From such aspects as reliability and economics, the dynamic environment is a major factor considered in choosing a launch vehicle. As vibration isolation is a useful structural control technique for improving the dynamic environment, the idea of WSVI is drawing more and more attention around the world. The concept of WSVI has been worked on since 1993, to date, at least six successful flights of different WSVI systems have been completed [9–12].

For the WSVI, a challenging problem is that a lower longitudinal stiffness is expected, which will introduce low-frequency bending modes of the spacecraft and result in a large lateral displacement of its top. This may increase the possibility of the collision between the spacecraft and the fairing. To restrict the lateral displacement, following the study of the octo-strut platform, an approach of stiffness design is developed to reinforce the rotation stiffness of the platform. Reliability is another major concern of the WSVI. To examine its capability of providing redundancy, the platform with one or two failed struts is also studied in the present paper.

2. Dynamic model of an octo-strut passive vibration isolation platform

A typical octo-strut vibration isolation platform (Fig. 1) consists of a base, a payload-interface and eight struts whose length varies along their axial direction. Although there are a number of strut models available, since the aim here is to investigate properties of the whole octo-strut platform, for the sake of convenience [5–8], the strut is simplified as a spring paralleled with a damper (Fig. 2). Connections of a strut to the base and the payload-interface are spherical joints. By neglecting the gravity and the inertial force of the strut, all forces transmitted through a strut are axial forces. This means that for a single strut, the vibration isolation is only in a single-axis

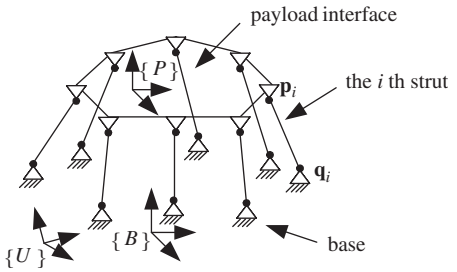

Fig. 1. A general octo-strut vibration isolation platform.

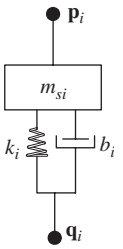

Fig. 2. The schematic of the ith strut.

direction. This helps to simplify the design of a single strut and further the whole vibration isolation platform design.

Three Cartesian reference frames are used here. $\{P\}$ is a reference frame rigidly attached to the payload-interface. $\{B\}$ is a reference frame rigidly attached to the base, and $\{U\}$ is a universal inertial reference frame. For a position, velocity or acceleration vector, a letter at the top left corner of it indicates the frame, relative to the origin of which the vector is measured, and for the other vector or tensor, the letter indicates the reference frame in which its matrix form is expressed.

Let $\mathbf{l}$ denote the vector of strut length, $\mathbf{l} = [l_1\ l_2\ \cdots\ l_N]^{\mathrm{T}}$, where N is the number of the struts. For the octo-strut platform, $N = 8$. l_i and l_{ri} are, respectively, the instantaneous length and the relaxed length of the ith strut. $\mathbf{x}_P$ is the displacement and attitude of the payload-interface, $\mathbf{x}_P = [\mathbf{P}_{P_{\mathrm{ORG}}}\ \boldsymbol{\Phi}]^{\mathrm{T}}$, $\mathbf{P}_{P_{\mathrm{ORG}}}$ is the position of the origin of $\{P\}$, $\boldsymbol{\Phi}$ is the Cardan angle that represents the attitude of the payload-interface, $\boldsymbol{\Phi} = [\theta_x\ \theta_y\ \theta_z]^{\mathrm{T}}$. Let ${}^{B}\mathbf{J}$ denote the Jacobian matrix that relates the elongation velocities of the struts, $\dot{\mathbf{l}}$, with the velocity of $\{P\}$ with respect to $\{B\}$, ${}^{B}\dot{\mathbf{x}}_P$. Then

$$\dot{\mathbf{l}} = {}^{B}\mathbf{J}\,{}^{B}\dot{\mathbf{x}}_P, \tag{1}$$

where $\dot{\mathbf{x}}_P = [\mathbf{v}_P\ \boldsymbol{\omega}_P]^{\mathrm{T}}$, $\mathbf{v}_P$ and $\boldsymbol{\omega}_P$ are, respectively, the velocity and the angular velocity of the payload-interface. Let $\mathbf{p}_i$ denote the position of the point connecting the payload-interface and the ith strut, and $\mathbf{q}_i$ denote the position of the point connecting the base and the ith strut. By defining a vector $\mathbf{w}_i = \mathbf{p}_i - \mathbf{q}_i$, the strut length is $l_i = \|\mathbf{w}_i\|$, and the unit vector along the axis of the ith strut is $\mathbf{u}_i = \mathbf{w}_i/l_i$. The expression of ${}^{B}\mathbf{J}$ can be obtained by expressing the absolute velocity at $\mathbf{p}_i$, $\mathbf{v}_{pi}$,

and projecting it along $\mathbf{u}_i$, that is

$$\dot{l}_i = {}^B\mathbf{u}_i \cdot {}^B\mathbf{v}_{pi} = {}^B\mathbf{u}_i \cdot [{}^B\mathbf{v}_P + {}^B\boldsymbol{\omega}_P \times ({}^B_P\mathbf{R}\,{}^P\mathbf{q}_i + l_i\,{}^B\mathbf{u}_i)], \tag{2}$$

where ${}^B_P\mathbf{R}$ is the transformation matrix from $\{P\}$ to $\{B\}$. Then

$$\dot{l}_i = {}^B\mathbf{u}_i \cdot {}^B\mathbf{v}_P + {}^B\mathbf{u}_i \cdot {}^B\boldsymbol{\omega}_P \times ({}^B_P\mathbf{R}\,{}^P\mathbf{q}_i) = {}^B\mathbf{u}_i \cdot {}^B\mathbf{v}_P + {}^B_P\mathbf{R}\,{}^P\mathbf{q}_i \times {}^B\mathbf{u}_i \cdot {}^B\boldsymbol{\omega}_P. \tag{3}$$

For all the struts, there is

$$\dot{\mathbf{l}} = {}^B\mathbf{J}\,{}^B\dot{\mathbf{x}}_P = \begin{pmatrix} {}^B\mathbf{u}_1^{\mathrm{T}} & \mathbf{s}_1^{\mathrm{T}} \\ {}^B\mathbf{u}_i^{\mathrm{T}} & \mathbf{s}_i^{\mathrm{T}} \\ {}^B\mathbf{u}_N^{\mathrm{T}} & \mathbf{s}_N^{\mathrm{T}} \end{pmatrix} \begin{pmatrix} {}^B\mathbf{v}_P \\ {}^B\boldsymbol{\omega}_P \end{pmatrix}, \tag{4}$$

where $\mathbf{s}_i = {}^B_P\mathbf{R}\,{}^P\mathbf{q}_i \times {}^B\mathbf{u}_i$. Let $\mathbf{F}_s$ denote the generalized force (including the force and the moment) acting on the payload-interface applied by all struts. f_{pi} denotes the axial force acting on the ith strut applied by the payload-interface, $\mathbf{f}_p = [f_{p1}, f_{p2}, \ldots, f_{pN}]^{\mathrm{T}}$. According to the balance equation of force or the virtual work theorem, there is

$${}^U\mathbf{F}_s = {}^U\mathbf{J}^{\mathrm{T}}\mathbf{f}_p = {}^U_B\mathbf{R}\,{}^B\mathbf{J}^{\mathrm{T}}\mathbf{f}_p, \tag{5}$$

where ${}^U_B\mathbf{R}$ is the transformation matrix from $\{B\}$ to $\{U\}$. It is used interchangeably (depending on dimension) to denote either a single 3×3 transformation matrix or two identical diagonally stacked 3×3 matrices forming a 6×6 matrix.

Fig. 2 illustrates the ith strut, where m_{si}, b_i and k_i are, respectively, the moving strut mass, the damping constant and the mount stiffness. Applying Newton's second law and stacking the equation into a vector form [7], there is

$$\mathbf{f}_p = -\mathbf{M}_s\ddot{\mathbf{l}} - \mathbf{B}\dot{\mathbf{l}} - \mathbf{K}(\mathbf{l} - \mathbf{l}_r) - \mathbf{M}_s\ddot{\mathbf{q}}_u - \mathbf{M}_s\mathbf{g}_u + \mathbf{M}_s\mathbf{a}_c, \tag{6}$$

where

$$\mathbf{f}_p = [f_{p1}\ f_{p2}\ \cdots\ f_{pN}]^{\mathrm{T}}, \quad \mathbf{l}_r = [l_{r1}\ l_{r2}\ \cdots\ l_{rN}]^{\mathrm{T}},$$

$$\mathbf{M}_s = \mathrm{diag}([m_{s1}\ m_{s2}\ \cdots\ m_{sN}]), \quad \mathbf{B} = \mathrm{diag}([b_1\ b_2\ \cdots\ b_N]),$$

$$\mathbf{K} = \mathrm{diag}([k_1\ k_2\ \cdots\ k_N]), \quad \mathbf{q}_u = [\mathbf{u}_1\mathbf{q}_1\ \mathbf{u}_2\mathbf{q}_2\ \cdots\ \mathbf{u}_N\mathbf{q}_N]^{\mathrm{T}},$$

$$\mathbf{g}_u = [\mathbf{u}_1\mathbf{g}\ \mathbf{u}_2\mathbf{g}\ \cdots\ \mathbf{u}_N\mathbf{g}]^{\mathrm{T}}, \quad \mathbf{g} \text{ is gravity acceleration vector},$$

$$\mathbf{a}_c = [\ddot{\mathbf{u}}_1\mathbf{w}_1 + 2\dot{\mathbf{u}}_1\dot{\mathbf{w}}_1\ \ddot{\mathbf{u}}_2\mathbf{w}_2 + 2\dot{\mathbf{u}}_2\dot{\mathbf{w}}_2\ \cdots\ \ddot{\mathbf{u}}_N\mathbf{w}_N + 2\dot{\mathbf{u}}_N\dot{\mathbf{w}}_N]^{\mathrm{T}}.$$

McInroy [7] and McInroy et al. [8] have developed the dynamic model of a Stewart platform with base acceleration. Here the dynamic model of an octo-strut platform with base acceleration is developed for whole-spacecraft passive vibration isolation. Assume that the Payload-Interface and the Payload (PIP) are rigidly attached, and they are modeled together as one rigid body. Its dynamic equation can be derived from Newton–Euler

dynamic formulation,

$$ {}^{U}\mathbf{F} = {}^{U}\mathbf{M}\,{}^{U}\ddot{\mathbf{x}}_P + \mathbf{c}({}^{U}\boldsymbol{\omega}_P), \tag{7} $$

where $\mathbf{F}$ and $\mathbf{M}$, respectively, indicate the generalized force acting on the PIP and the mass/inertia matrix of the PIP. Let m, $\mathbf{I}_3$ and ${}^{U}\mathbf{I}$, respectively, denote the mass of the PIP, the three-order identity matrix and the inertia matrix of the PIP, then

$$ {}^{U}\mathbf{M} = \begin{bmatrix} m\mathbf{I}_3 & \mathbf{0}_{3\times 3} \\ \mathbf{0}_{3\times 3} & {}^{U}\mathbf{I} \end{bmatrix}. \tag{8} $$

In Eq. (7), $\ddot{\mathbf{x}}_P$ is the generalized acceleration of the PIP and $\mathbf{c}({}^{U}\boldsymbol{\omega}_P)$ denotes the vector of Coriolis and centripetal terms.

The total generalized force acting on the PIP is

$$ {}^{U}\mathbf{F} = {}^{U}\mathbf{F}_s + [m^{U}\mathbf{g}\ \mathbf{0}_{3\times 1}]^{\mathrm{T}} + {}^{U}\mathbf{F}_e, \tag{9} $$

where $\mathbf{F}_e$ represents the exogenous generalized force acting on the PIP except the gravity and $\mathbf{F}_s$. From Eqs. (5)–(7) and (9), there is

$$ \begin{aligned} &{}^{U}\mathbf{J}^{\mathrm{T}}[-\mathbf{M}_s\ddot{\mathbf{l}} - \mathbf{B}\dot{\mathbf{l}} - \mathbf{K}(\mathbf{l}-\mathbf{l}_r) - \mathbf{M}_s\ddot{\mathbf{q}}_u - \mathbf{M}_s\mathbf{g}_u + \mathbf{M}_s\mathbf{a}_c] + [m^{U}\mathbf{g}\ \mathbf{0}_{3\times 1}]^{\mathrm{T}} + {}^{U}\mathbf{F}_e \\ &\quad = {}^{U}\mathbf{M}\,{}^{U}\ddot{\mathbf{x}}_P + \mathbf{c}({}^{U}\boldsymbol{\omega}_P). \end{aligned} \tag{10} $$

To get dynamic properties of the system in the Cartesian space, $\ddot{\mathbf{l}}$, $\dot{\mathbf{l}}$, $(\mathbf{l}-\mathbf{l}_r)$ and $\ddot{\mathbf{q}}_u$ should be substituted with ${}^{U}\mathbf{x}_P$ and ${}^{U}\mathbf{x}_B$, or their derivatives, where $\mathbf{x}_B$ denotes the position and attitude of $\{B\}$.

In the universal inertial frame, ${}^{U}\mathbf{q}_i = {}^{U}_{B}\mathbf{R}\,{}^{B}\mathbf{q}_i + {}^{U}\mathbf{P}_{B_{\mathrm{ORG}}}$, where $\mathbf{P}_{B_{\mathrm{ORG}}}$ is the position of the origin of $\{B\}$. Its twice differentiation yields

$$ {}^{U}\ddot{\mathbf{q}}_i = {}^{U}\dot{\boldsymbol{\omega}}_B \times {}^{U}_{B}\mathbf{R}\,{}^{B}\mathbf{q}_i + {}^{U}\dot{\mathbf{v}}_B + {}^{U}\boldsymbol{\omega}_B \times ({}^{U}\boldsymbol{\omega}_B \times {}^{U}_{B}\mathbf{R}\,{}^{B}\mathbf{q}_i), \tag{11} $$

where $\boldsymbol{\omega}_B$ and $\mathbf{v}_B$, respectively, denote the angular velocity and the velocity of $\{B\}$, $\mathbf{v}_B = \dot{\mathbf{P}}_{B_{\mathrm{ORG}}}$. A matrix form of Eq. (11) is

$$ {}^{U}\mathbf{u}_i\,{}^{U}\ddot{\mathbf{q}}_i = [{}^{U}\mathbf{u}_i\ {}^{U}_{B}\mathbf{R}\,{}^{B}\mathbf{q}_i \times {}^{U}\mathbf{u}_i]\,{}^{U}\ddot{\mathbf{x}}_B + {}^{U}\mathbf{u}_i({}^{U}\boldsymbol{\omega}_B \times ({}^{U}\boldsymbol{\omega}_B \times {}^{U}_{B}\mathbf{R}\,{}^{B}\mathbf{q}_i)), \tag{12} $$

where $\ddot{\mathbf{x}}_B = [\dot{\mathbf{v}}_B\ \dot{\boldsymbol{\omega}}_B]^{\mathrm{T}}$. Integrating equations of all struts together, we obtain

$$ \ddot{\mathbf{q}}_u = \mathbf{J}_B\,{}^{U}\ddot{\mathbf{x}}_B + \mathbf{c}_B, \tag{13} $$

where

$$ \mathbf{J}_B = \begin{bmatrix} {}^{U}\mathbf{u}_1 & {}^{U}_{B}\mathbf{R}\,{}^{B}\mathbf{q}_1 \times {}^{U}\mathbf{u}_1 \\ \vdots & \vdots \\ {}^{U}\mathbf{u}_N & {}^{U}_{B}\mathbf{R}\,{}^{B}\mathbf{q}_N \times {}^{U}\mathbf{u}_N \end{bmatrix}, \quad \mathbf{c}_B = \begin{bmatrix} {}^{U}\mathbf{u}_1^{\mathrm{T}}({}^{U}\boldsymbol{\omega}_B \times ({}^{U}\boldsymbol{\omega}_B \times {}^{U}_{B}\mathbf{R}\,{}^{B}\mathbf{q}_1)) \\ \vdots \\ {}^{U}\mathbf{u}_N^{\mathrm{T}}({}^{U}\boldsymbol{\omega}_B \times ({}^{U}\boldsymbol{\omega}_B \times {}^{U}_{B}\mathbf{R}\,{}^{B}\mathbf{q}_N)) \end{bmatrix}. $$

Note that $\mathbf{J}_B$ is identical in form to ${}^{B}\mathbf{J}$, but it relates the acceleration at $\mathbf{q}_i$ along axial direction of the strut to the acceleration of $\{B\}$ with respect to $\{U\}$.

The position of the origin of $\{P\}$ with respect to $\{U\}$ is ${}^{U}\mathbf{P}_{P_{\mathrm{ORG}}} = {}^{U}_{B}\mathbf{R}\,{}^{B}\mathbf{P}_{P_{\mathrm{ORG}}} + {}^{U}\mathbf{P}_{B_{\mathrm{ORG}}}$. Considering $\mathbf{v}_P = \dot{\mathbf{P}}_{P_{\mathrm{ORG}}}$, its differentiation yields

$$ {}^{U}\mathbf{v}_P = {}^{U}_{B}\mathbf{R}\,{}^{B}\mathbf{v}_P + {}^{U}\mathbf{v}_B + {}^{U}\boldsymbol{\omega}_B \times {}^{U}_{B}\mathbf{R}\,{}^{B}\mathbf{P}_{P_{\mathrm{ORG}}}, \tag{14} $$

$$ {}^{U}\dot{\mathbf{v}}_P = {}^{U}_{B}\mathbf{R}\,{}^{B}\dot{\mathbf{v}}_P + {}^{U}\dot{\mathbf{v}}_B - {}^{U}_{B}\mathbf{R}\,{}^{B}\mathbf{P}_{P_{\mathrm{ORG}}} \times {}^{U}\dot{\boldsymbol{\omega}}_B + 2\,{}^{U}\boldsymbol{\omega}_B \times {}^{U}_{B}\mathbf{R}\,{}^{B}\mathbf{v}_P + {}^{U}\boldsymbol{\omega}_B \times ({}^{U}\boldsymbol{\omega}_B \times {}^{U}_{B}\mathbf{R}\,{}^{B}\mathbf{P}_{P_{\mathrm{ORG}}}). \tag{15} $$

The angular velocity of the PIP with respect to $\{U\}$ and its differentiation are

$$ {}^{U}\boldsymbol{\omega}_P = {}^{U}_{B}\mathbf{R}\,{}^{B}\boldsymbol{\omega}_P + {}^{U}\boldsymbol{\omega}_B, \tag{16} $$

$$ {}^{U}\dot{\boldsymbol{\omega}}_P = {}^{U}_{B}\mathbf{R}\,{}^{B}\dot{\boldsymbol{\omega}}_P + {}^{U}\dot{\boldsymbol{\omega}}_B + {}^{U}\boldsymbol{\omega}_B \times {}^{U}_{B}\mathbf{R}\,{}^{B}\boldsymbol{\omega}_P. \tag{17} $$

Integrating Eqs. (14)–(17), we obtain

$$ {}^{U}\dot{\mathbf{x}}_P = {}^{U}_{B}\mathbf{R}\,{}^{B}\dot{\mathbf{x}}_P + \begin{bmatrix} \mathbf{I} & -({}^{U}_{B}\mathbf{R}\,{}^{B}\mathbf{P}_{P_{\mathrm{ORG}}})\times \\ 0 & \mathbf{I} \end{bmatrix} {}^{U}\dot{\mathbf{x}}_B, \tag{18} $$

$$ \begin{aligned} {}^{U}\ddot{\mathbf{x}}_P = {}^{U}_{B}\mathbf{R}\,{}^{B}\ddot{\mathbf{x}}_P + \begin{bmatrix} \mathbf{I} & -({}^{U}_{B}\mathbf{R}\,{}^{B}\mathbf{P}_{P_{\mathrm{ORG}}})\times \\ \mathbf{0} & \mathbf{I} \end{bmatrix} {}^{U}\ddot{\mathbf{x}}_B \\ + \begin{bmatrix} 2\,{}^{U}\boldsymbol{\omega}_B \times {}^{U}_{B}\mathbf{R}\,{}^{B}\mathbf{v}_P + {}^{U}\boldsymbol{\omega}_B \times ({}^{U}\boldsymbol{\omega}_B \times {}^{U}_{B}\mathbf{R}\,{}^{B}\mathbf{P}_{P_{\mathrm{ORG}}}) \\ {}^{U}\boldsymbol{\omega}_B \times {}^{U}_{B}\mathbf{R}\,{}^{B}\boldsymbol{\omega}_P \end{bmatrix} \end{aligned} \tag{19} $$

or in compact forms as

$$ {}^{U}\dot{\mathbf{x}}_P = {}^{U}_{B}\mathbf{R}\,{}^{B}\dot{\mathbf{x}}_P + \mathbf{J}_c\,{}^{U}\dot{\mathbf{x}}_B, \tag{20} $$

$$ {}^{U}\ddot{\mathbf{x}}_P = {}^{U}_{B}\mathbf{R}\,{}^{B}\ddot{\mathbf{x}}_P + \mathbf{J}_c\,{}^{U}\ddot{\mathbf{x}}_B + \mathbf{c}_{PB}. \tag{21} $$

Differentiating Eq. (4) yields

$$ \ddot{\mathbf{l}} = {}^{B}\mathbf{J}\,{}^{B}\ddot{\mathbf{x}}_P + {}^{B}\dot{\mathbf{J}}\,{}^{B}\dot{\mathbf{x}}_P. \tag{22} $$

Substitute Eqs. (4), (13), (21) and (22) into Eq. (10),

$$ \begin{aligned} &({}^{U}\mathbf{M}\,{}^{U}_{B}\mathbf{R} + {}^{U}\mathbf{J}^{\mathrm{T}}\mathbf{M}_s\,{}^{B}\mathbf{J})\,{}^{B}\ddot{\mathbf{x}}_P + {}^{U}\mathbf{J}^{\mathrm{T}}\mathbf{B}\,{}^{B}\mathbf{J}\,{}^{B}\dot{\mathbf{x}}_P + {}^{U}\mathbf{J}^{\mathrm{T}}\mathbf{K}(\mathbf{l}-\mathbf{l}_r) \\ &\quad = -({}^{U}\mathbf{M}\mathbf{J}_C + {}^{U}\mathbf{J}^{\mathrm{T}}\mathbf{M}_s\mathbf{J}_B)\,{}^{U}\ddot{\mathbf{x}}_B + {}^{U}\mathbf{F}_e + \mathbf{G} + \mathbf{C}, \end{aligned} \tag{23} $$

where $\mathbf{G}$ contains all gravity terms, and $\mathbf{C}$ contains all Coriolis and centripetal terms.

By assuming that the vibration amplitude is sufficiently small, ${}^{U}_{B}\mathbf{R}$, $\mathbf{G}$, $\mathbf{J}$, $\mathbf{J}_c$ and $\mathbf{J}_B$ are constants, and the velocity is a small quantity, the two-order small quantities can be discarded, thus $\mathbf{C} \approx \mathbf{0}$, $\mathbf{c}_B \approx \mathbf{0}$, $\mathbf{c}_{PB} \approx \mathbf{0}$ and $(\mathbf{l}-\mathbf{l}_r) \approx {}^{B}\mathbf{J}\,{}^{B}\mathbf{x}_P$. $\mathbf{M}_s$ can also be omitted if ${}^{U}\mathbf{J}^{\mathrm{T}}\mathbf{M}_s\,{}^{U}\mathbf{J} \ll {}^{U}\mathbf{M}$. If the spring compression balances the gravity force, the gravity term $\mathbf{G}$ can also be removed. With these approximations and conditions, Eq. (23) can be simplified as

$$ {}^{U}\mathbf{M}\,{}^{U}_{B}\mathbf{R}\,{}^{B}\ddot{\mathbf{x}}_P + {}^{U}\mathbf{J}^{\mathrm{T}}\mathbf{B}\,{}^{B}\mathbf{J}\,{}^{B}\dot{\mathbf{x}}_P + {}^{U}\mathbf{J}^{\mathrm{T}}\mathbf{K}\,{}^{B}\mathbf{J}\,{}^{B}\mathbf{x}_P = -{}^{U}\mathbf{M}\mathbf{J}_C\,{}^{U}\ddot{\mathbf{x}}_B + {}^{U}\mathbf{F}_e. \tag{24} $$

Introducing Eqs. (20) and (21) into Eq. (24), the above equation has the form as

$$ {}^{U}\mathbf{M}\,{}^{U}\ddot{\mathbf{x}}_P + {}^{U}\mathbf{J}^{\mathrm{T}}\mathbf{B}\,{}^{U}\mathbf{J}({}^{U}\dot{\mathbf{x}}_P - \mathbf{J}_C\,{}^{U}\dot{\mathbf{x}}_B) + {}^{U}\mathbf{J}^{\mathrm{T}}\mathbf{K}\,{}^{U}\mathbf{J}({}^{U}\mathbf{x}_P - {}^{U}\mathbf{x}_B) = {}^{U}\mathbf{F}_e. \tag{25} $$

Let $\mathbf{B}_{\mathrm{platform}} = {}^{U}\mathbf{J}^{\mathrm{T}}\mathbf{B}\,{}^{U}\mathbf{J}$, $\mathbf{K}_{\mathrm{platform}} = {}^{U}\mathbf{J}^{\mathrm{T}}\mathbf{K}\,{}^{U}\mathbf{J}$, and ${}^{U}\mathbf{F}_e = 0$, the transmissibility matrix from the base to the PIP can be written as

$$ \mathbf{T}(s) = {}^{U}\mathbf{x}_P(s)\,{}^{U}\mathbf{x}_B(s)^{-1} = ({}^{U}\mathbf{M}s^2 + \mathbf{B}_{\mathrm{platform}}s + \mathbf{K}_{\mathrm{platform}})^{-1}(\mathbf{B}_{\mathrm{platform}}\mathbf{J}_C s + \mathbf{K}_{\mathrm{platform}}). \tag{26} $$

In the above analysis, the number of strut is eight, namely $N = 8$. In fact, the above analysis procedure is applicable to any case that $N \geqslant 6$.

3. Stiffness design

Because the mechanical interfaces of the launch vehicle and the spacecraft are symmetric and circular, it is recommended that the isolation platform should be also a symmetric structure (Fig. 3) that joint points are symmetrically arranged on two connecting rings with respect to x- and y-axis of $\{P\}$. Increasing rotation stiffness but not augmenting the longitudinal stiffness is a great challenge of the platform design. With such a symmetric structure, this challenge can be defeated by a proper stiffness design. An approach is to take the advantage of coupling stiffness.

To further simplify the design and analysis of the platform, all struts are assumed to have same dynamic properties, and the three coordinate frames are selected to point to the same directions as the principal axes of inertial of the payload. Under such conditions, rotation matrix, ${}^{U}_{B}\mathbf{R}$ is an identity matrix, ${}^{U}\mathbf{J} = {}^{B}\mathbf{J}$, and ${}^{U}\mathbf{M}_x$ is a diagonal matrix. To concentrate the discussion on the stiffness design, terms of damping and excitations in Eq. (25) are omitted, and thus the equation is turned into

$$ {}^{U}\mathbf{M}\,{}^{U}\ddot{\mathbf{x}}_P + \mathbf{K}_{\mathrm{platform}}\,{}^{U}\mathbf{x}_P = 0. \tag{27} $$

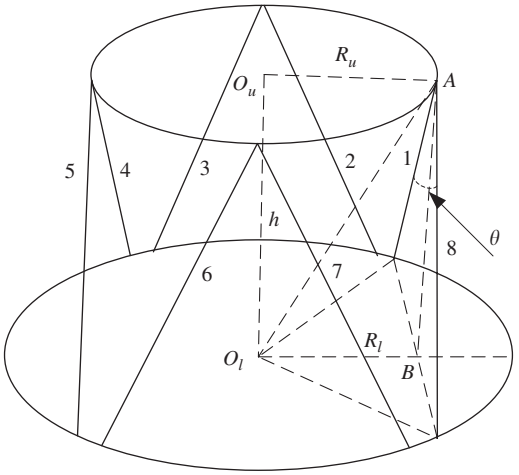

Fig. 3. The geometry schematic of the symmetric octo-strut vibration isolation platform.

According to Eq. (4),

$$\mathbf{K}_{\text{platform}} = \begin{bmatrix} \mathbf{u}_1 & \mathbf{u}_2 & \cdots & \mathbf{u}_N \\ \mathbf{s}_1 & \mathbf{s}_2 & \cdots & \mathbf{s}_N \end{bmatrix} \begin{bmatrix} k & 0 & \cdots & 0 \\ 0 & k & \cdots & 0 \\ \vdots & \vdots & \ddots & 0 \\ 0 & 0 & \cdots & k \end{bmatrix} \begin{bmatrix} \mathbf{u}_1^{\mathrm{T}} & \mathbf{s}_1^{\mathrm{T}} \\ \mathbf{u}_2^{\mathrm{T}} & \mathbf{s}_2^{\mathrm{T}} \\ \vdots & \vdots \\ \mathbf{u}_N^{\mathrm{T}} & \mathbf{s}_N^{\mathrm{T}} \end{bmatrix}$$

$$= k \begin{bmatrix} \sum_{i=1}^{N} \mathbf{u}_i \mathbf{u}_i^{\mathrm{T}} & \sum_{i=1}^{N} \mathbf{u}_i \mathbf{s}_i^{\mathrm{T}} \\ \sum_{i=1}^{N} \mathbf{s}_i \mathbf{u}_i^{\mathrm{T}} & \sum_{i=1}^{N} \mathbf{s}_i \mathbf{s}_i^{\mathrm{T}} \end{bmatrix}. \tag{28}$$

Let $\mathbf{p}_i = [p_{ix}\ p_{iy}\ p_{iz}]^{\mathrm{T}}$, $\mathbf{q}_i = [q_{ix}\ q_{iy}\ q_{iz}]^{\mathrm{T}}$, $\mathbf{u}_i = [u_{i1}\ u_{i2}\ u_{i3}]^{\mathrm{T}}$, $\mathbf{s}_i = [s_{i1}\ s_{i2}\ s_{i3}]^{\mathrm{T}}$. From the structural symmetry, more relations among coordinates of joint points can be derived as

$$\sum_{i=1}^{N} p_{ix} = \sum_{i=1}^{N} p_{iy} = \sum_{i=1}^{N} q_{ix} = \sum_{i=1}^{N} q_{iy} = \sum_{i=1}^{N} p_{ix}p_{iy} = \sum_{i=1}^{N} q_{ix}q_{iy} = \sum_{i=1}^{N} p_{ix}q_{iy} = 0, \tag{29}$$

$$p_{1z} = p_{2z} = \cdots = p_{Nz}, \quad q_{1z} = q_{2z} = \cdots = q_{Nz}. \tag{30}$$

With the definitions of $\mathbf{u}_i$ and $\mathbf{s}_i$, these relations result in

$$\sum_{i=1}^{N} u_{ik}u_{il} = \sum_{i=1}^{N} s_{ik}s_{il} = \sum_{i=1}^{N} u_{ik}s_{il} = 0, \quad k \text{ or } l = 3 \text{ and } k \neq l,$$

$$\sum_{i=1}^{N} u_{i1}u_{i2} = 0,\ \sum_{i=1}^{N} s_{i1}s_{i2} = 0,\ \sum_{i=1}^{N} u_{i1}s_{i1} = 0,\ \sum_{i=1}^{N} u_{i2}s_{i2} = 0,\ \sum_{i=1}^{N} u_{i3}s_{i3} = 0. \tag{31}$$

Then Eq. (28) can be turned into

$$\mathbf{K}_{\text{platform}} = k \begin{bmatrix} \sum_{i=1}^{N} u_{i1}^2 & 0 & 0 & 0 & \sum_{i=1}^{N} u_{i1}s_{i2} & 0 \\ 0 & \sum_{i=1}^{N} u_{i2}^2 & 0 & \sum_{i=1}^{N} u_{i2}s_{i1} & 0 & 0 \\ 0 & 0 & \sum_{i=1}^{N} u_{i3}^2 & 0 & 0 & 0 \\ 0 & \sum_{i=1}^{N} s_{i1}u_{i2} & 0 & \sum_{i=1}^{N} s_{i1}^2 & 0 & 0 \\ \sum_{i=1}^{N} s_{i2}u_{i1} & 0 & 0 & 0 & \sum_{i=1}^{N} s_{i2}^2 & 0 \\ 0 & 0 & 0 & 0 & 0 & \sum_{i=1}^{N} s_{i3}^2 \end{bmatrix}. \tag{32}$$

From the above stiffness matrix of the platform, it can be seen that the z-direction stiffness does not couple with those of other degrees of freedom (dofs). Because ${}^{U}\mathbf{M}$ is also a diagonal matrix, the z-direction dynamic equation in Eq. (27) are independent from other dofs.

With an octo-strut platform (Fig. 3) as an example, adding coupling stiffness between strut 1 and 5, 2 and 6, 3 and 7, 4 and 8, the stiffness matrix of all struts, $\mathbf{K}$, is expressed as

$$\mathbf{K}=\begin{bmatrix} k+k_c & 0 & 0 & 0 & -k_c & 0 & 0 & 0 \\ 0 & k+k_c & 0 & 0 & 0 & -k_c & 0 & 0 \\ 0 & 0 & k+k_c & 0 & 0 & 0 & -k_c & 0 \\ 0 & 0 & 0 & k+k_c & 0 & 0 & 0 & -k_c \\ -k_c & 0 & 0 & 0 & k+k_c & 0 & 0 & 0 \\ 0 & -k_c & 0 & 0 & 0 & k+k_c & 0 & 0 \\ 0 & 0 & -k_c & 0 & 0 & 0 & k+k_c & 0 \\ 0 & 0 & 0 & -k_c & 0 & 0 & 0 & k+k_c \end{bmatrix}, \tag{33}$$

where k_c is the coupling stiffness of two struts, which can be implemented by hydraulic link or special mechanism. Then the new stiffness matrix of the platform, $\mathbf{K}_{\text{platform}}$, becomes

$$\mathbf{K}_{\text{platform}} = \begin{bmatrix} (k+2k_c)\sum_{i=1}^{8} u_{i1}^2 & 0 & 0 & 0 & (k+2k_c)\sum_{i=1}^{8} u_{i1}s_{i2} & 0 \\ 0 & (k+2k_c)\sum_{i=1}^{8} u_{i2}^2 & 0 & (k+2k_c)\sum_{i=1}^{8} u_{i2}s_{i1} & 0 & 0 \\ 0 & 0 & k\sum_{i=1}^{8} u_{i3}^2 & 0 & 0 & 0 \\ 0 & (k+2k_c)\sum_{i=1}^{8} s_{i1}u_{i2} & 0 & (k+2k_c)\sum_{i=1}^{8} s_{i1}^2 & 0 & 0 \\ (k+2k_c)\sum_{i=1}^{8} s_{i2}u_{i1} & 0 & 0 & 0 & (k+2k_c)\sum_{i=1}^{8} s_{i2}^2 & 0 \\ 0 & 0 & 0 & 0 & 0 & k\sum_{i=1}^{8} s_{i3}^2 \end{bmatrix} \tag{34}$$

which keeps the same form as Eq. (32). Although the stiffness of z-direction and θ_z-direction is not changed, other nonzero elements in the matrix are increased by $2k_c$, namely rotation stiffness of the platform is increased. This also means that the nature frequencies of z-direction and θ_z-direction modes are kept the same, but frequencies corresponding to those bending modes are considerably increased.

In Eq. (25), $\mathbf{B}_{\text{platform}}$ has the same form as $\mathbf{K}_{\text{platform}}$. If reference frames $\{B\}$ and $\{P\}$ have same z-axis, namely ${}^{B}\mathbf{P}_{P_{\text{ORG}}} = [0\ 0\ z_p]^{\text{T}}$, the z-direction damping of the platform also has no coupling

with those of other dofs. Therefore, it is easy to determine the stiffness, k, and the damping, c, of a single strut from the break frequency and the damping ratio of the whole platform along the z-axis.

4. Numerical study

In this section, the performance of the octo-strut platform for the vibration isolation is numerically studied by coupling it with both rigid satellite and flexible satellite. This also serves as numerical examples to illustrate the above theory.

Parameters of the PIP are as the following: mass $m = 1387.455\,\text{kg}$, moment of inertia to the centroid $I_x = 702.1$, $I_y = 686.3$ and $I_z = 397.2\,\text{kg m}^2$, satellite height $H = 4\,\text{m}$, centroid height $H_c = 1.468\,\text{m}$. The structural parameters of the octo-strut platform (Fig. 3) are: up ring radius $R_u = 0.602\,\text{m}$, low ring radius $R_l = 0.856\,\text{m}$, platform height $h = 0.3\,\text{m}$, and included angle of a pair of struts $\theta = \pi/2$. Comparing with the mass of the satellite, the moving mass of the strut (about 1 kg) can be omitted. Assume that the required z-direction break frequency and the z-direction damping ratio of the platform are, respectively, 6.5 Hz and 0.19. According to the study in Section 3, the stiffness and the damping coefficient of a single strut can be found as 7.8541e + 005 N/m and 7.3078e + 003 kg/s.

4.1. Stiffness design

The nature frequencies of vibration isolation system with or without coupling stiffness are showed in Table 1. It is obvious that the frequencies of z-direction mode and θ_z-direction (z rotation) mode are constant. However, those frequencies with respect to x-direction rotation modes and y-direction rotation modes (namely bending modes) are significantly increased. This demonstrates the effectiveness of the method suggested in Section 3.

The satellite is subject to a maximum lateral acceleration load $3g$ ($g = 9.8\,\text{N m/s}^2$). Without the coupling stiffness, the lateral displacement of the top of the satellite is 0.851 m. By adding the coupling stiffness, this displacement is reduced to 0.0293 m, only 3.4% of the original amplitude.

4.2. Parameter analysis and optimization

The symmetric octo-strut platform is defined by four parameters. R_u and R_l are decided by the interface parameters of the spacecraft and the launch vehicle. Only θ and h can be chosen freely in their given ranges. Figs. 4–7 show the influences of these two parameters on the nature frequencies

Table 1
The nature frequencies (Hz) of the vibration isolation system with or without coupling stiffness

	k (N/m)	k_c (N/m)	z	z rotation	x rotation		y rotation	
Uncoupled	7.854e5	0	6.5	8.521	1.657	12.72	1.652	12.60
Coupled	7.854e5	2.1991e7	6.5	8.521	8.922	68.47	8.901	67.86

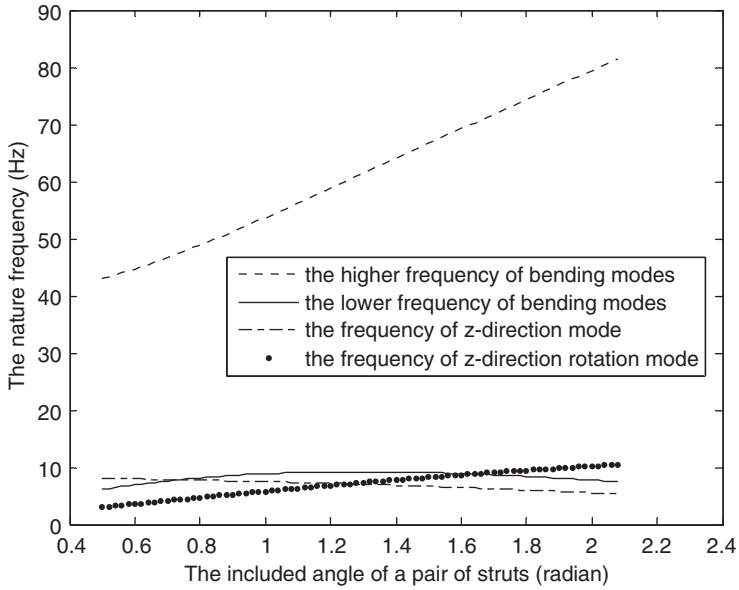

Fig. 4. The influence of the included angle of a pair of struts on nature frequencies.

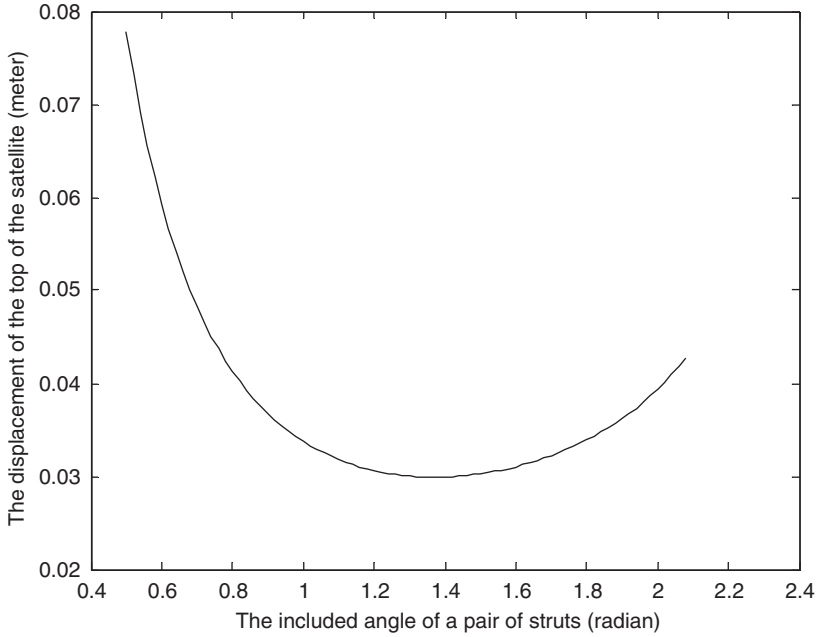

Fig. 5. The influence of the included angle of a pair of struts on the lateral displacement.

and the maximum lateral displacement of the top of the satellite. There are six nature frequencies of the whole system. As shown in Table 1, two pairs of frequencies of bending modes are nearly the same. So there are only four curves in Figs. 4 and 6. Fig. 4 indicates that when the included

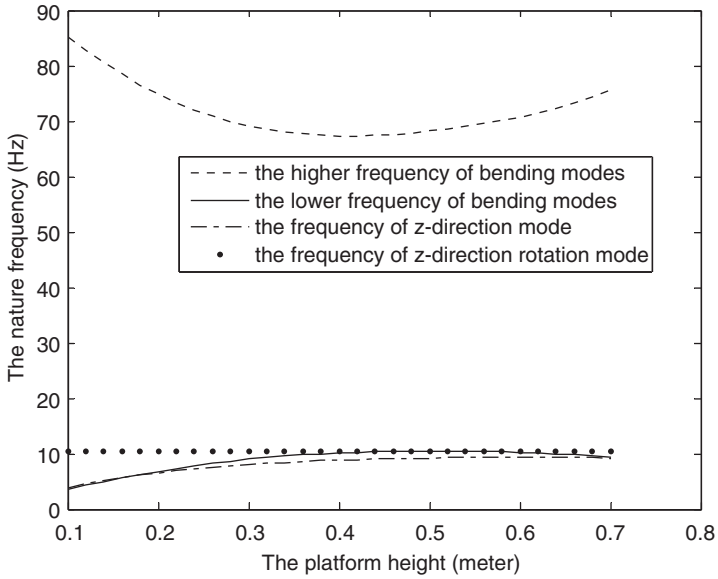

Fig. 6. The influence of the platform height on nature frequencies.

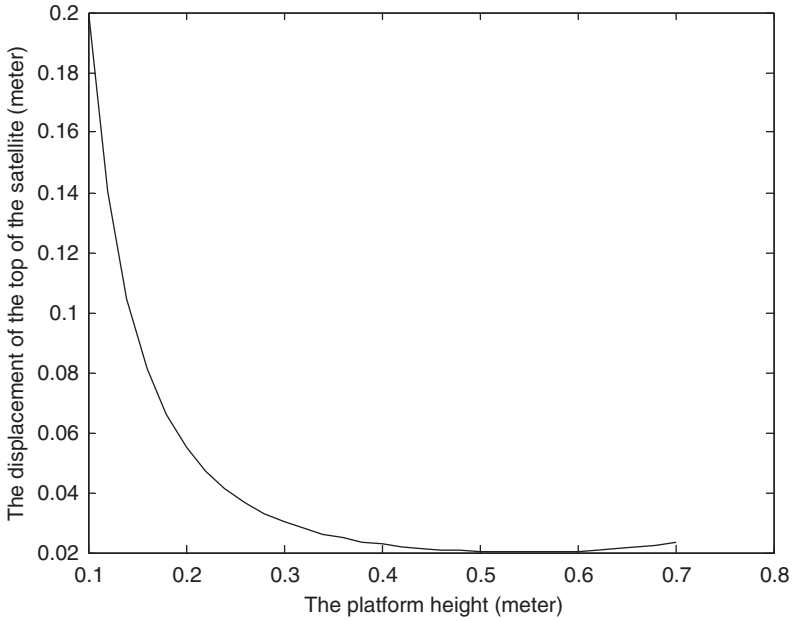

Fig. 7. The influence of the platform height on the lateral displacement.

angle increases, the frequency of rolling (z-direction rotation) mode and the higher frequency of bending modes also increase, but the frequency of z-direction mode decreases monotonously. The lower frequency of bending modes first increases and then decreases after a certain included angle. This angle is also a turning point for the lateral displacement of the top

of the satellite as shown in Fig. 5, but before which the lateral displacement first decreases and after which it increases. Fig. 6 indicates that the platform height have no effect on the frequency of rolling mode, but when it increases, the frequency of z-direction mode also increase, the lower frequency of bending modes first increases and then decreases, on the contrary, the higher frequency of bending modes first decreases and then increases. Fig. 7 shows that as the platform height increases, the lateral displacement of the top of the satellite also first decreases and then increases.

Figs. 5 and 7 also show that there exist an optimal included angle, θ, and an optimal platform height, h, which can minimize the lateral displacement of the top of the satellite. In the optimization procedure, θ and h are chosen as the optimal design parameters, Sequential Quadratic Programming (SQP) method is selected as the optimal algorithm, and the lateral displacement of the top of the satellite is used as the objective function. The constraint condition is that the longitudinal break frequency of the platform equals to 6.5 Hz, and any two struts should not interfere with each other, namely $|\mathbf{q}_1 - \mathbf{q}_2| > 0.1$. The optimal values of θ and h are finally obtained as 1.500 rad and 0.467 m, respectively. The lateral displacement is 0.0199 m. In order to add confidence that this result is a global minimum (or least a good minimum) one, the optimization is started with several groups of different initial design parameters and yields the similar result, which is a commonly used engineering approach [13].

4.3. Transmissibility with a rigid satellite

The aim of whole-spacecraft vibration isolation is to reduce the acceleration transmissibility from the top of the base of the platform to the satellite. Since the base disturbance has six dof input and the satellite has six dof output, the transmissibility from the base to the satellite is a 6×6 matrix. It can be illustrated by a matrix form figure (Fig. 8), in which labels of columns at the bottom of the figure depict the input direction, and labels of rows at the left-hand side of the figure depict the output direction. For example, the small figure at the third row and the third column depicts the transmissibility of z-direction input of the base and z-direction output of the satellite. Although some details are hard to be read on this crowded graph, it can show that the vibration in x-direction and θ_y-direction, y-direction and θ_x-direction are coupling, but the vibration in z-direction and θ_z-direction are uncoupling, which is consistent with the theory developed in Section 3.

The total root-mean-square (rms) response of the system with random excitation is usually as a standard index to the effectiveness of vibration isolation. Its expression is

$$\text{rms} = \sqrt{\int_{-\infty}^{\infty} |\mathbf{T}(\mathrm{j}\omega)|^2 S_x(\omega)\,\mathrm{d}\omega}, \tag{35}$$

where $S_x(\omega)$ is the input power spectrum. Fig. 9 presents the input acceleration power spectrum of the base and the output acceleration power spectrum of the satellite in z-direction. Total rms of the input power density of the base is $7.48g$ and that of the satellite is only $0.0476g$. This means the vibration platform is effective for the attenuation of random vibration.

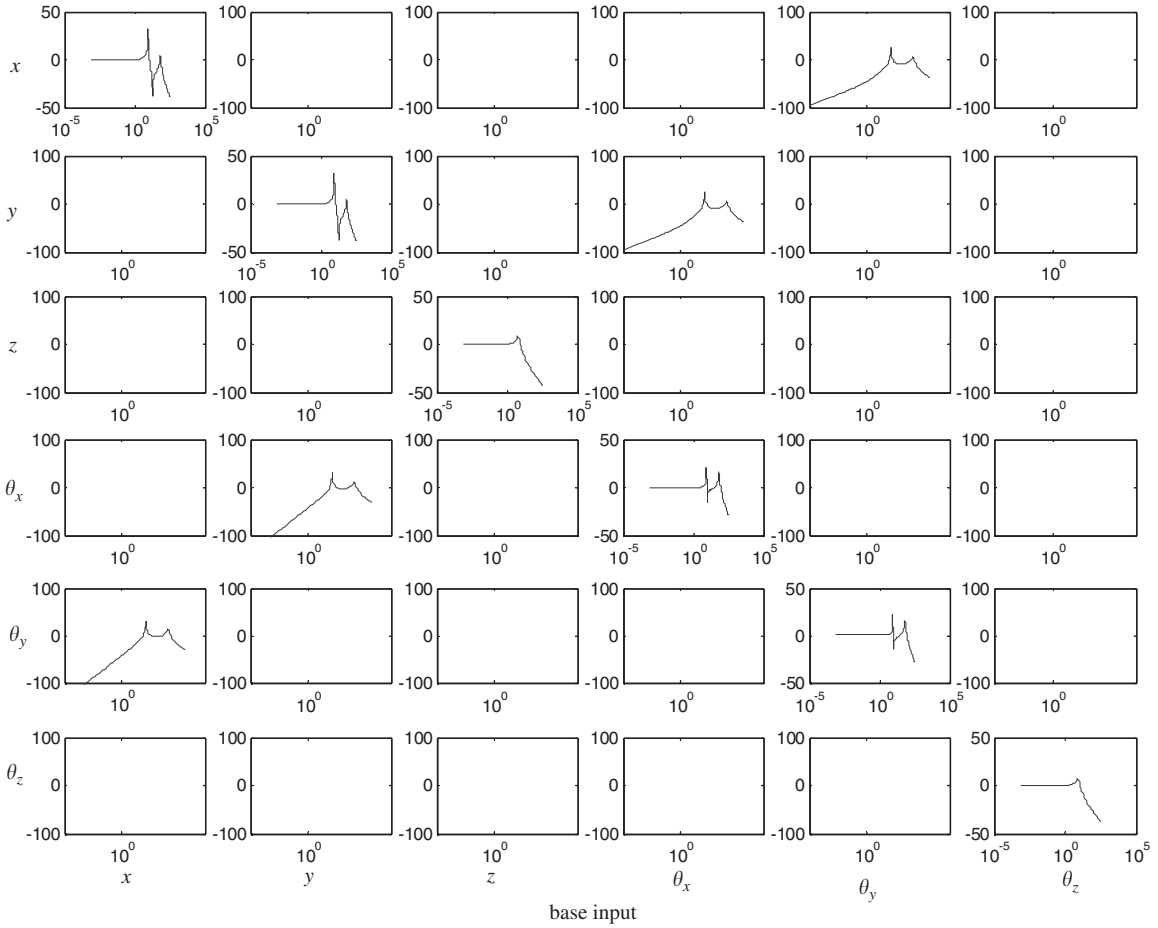

Fig. 8. The transmissibility from the base to the satellite.

4.4. Transmissibility with a flexible satellite

In fact, payload is generally a flexible body. To take the flexibility of a satellite into account, Finite Element Model (FEM) of a satellite (Fig. 10) is used. It is divided into two super-elements. The first super-element represents the part of the satellite above the second separation plane. The condensed stiffness matrix and mass matrix are derived by the fix-interface mode synthesis method. The fixed interface is the second separation plane that is simplified as a node with six dof. The second super-element is the cone-shaped joint component of the satellite with two interfaces, which are also simplified as two nodes each with six dof. The upper node is used to connect the first super-element, and the lower node is used to joint the payload-interface. The condensed stiffness matrix and mass matrix are also given by the fix-interface mode synthesis method. The maximum resonant frequency of this condensed model is below 120 Hz.

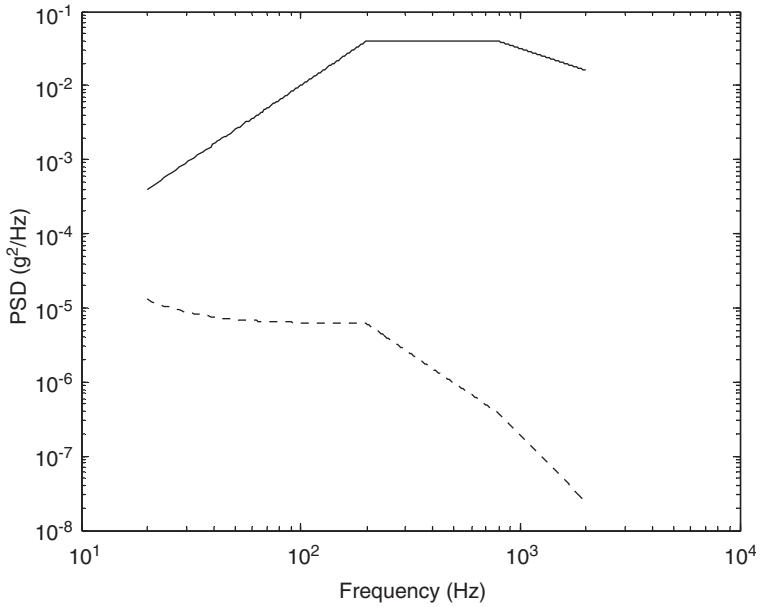

Fig. 9. The longitudinal input power density (total rms 7.48g) and longitudinal output power density (total rms 0.0476g).

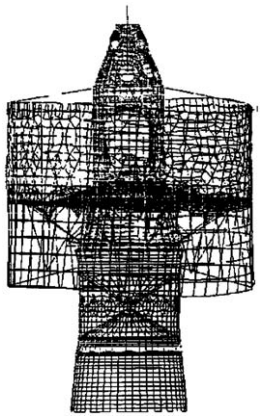

Fig. 10. The finite element model of a satellite.

Figs. 11 and 12 are the transmissibility of the octo-strut platform topped with this flexible satellite. In these figures, dashed line indicates the transmissibility from the bottom of the cone-shaped joint component to the divided plane without the isolator platform, and solid line shows the transmissibility from the bottom of the isolator platform to the divided plane. Because of the flexibility of the satellite, there are more peaks in the transmissibility curve than with the rigid satellite body.

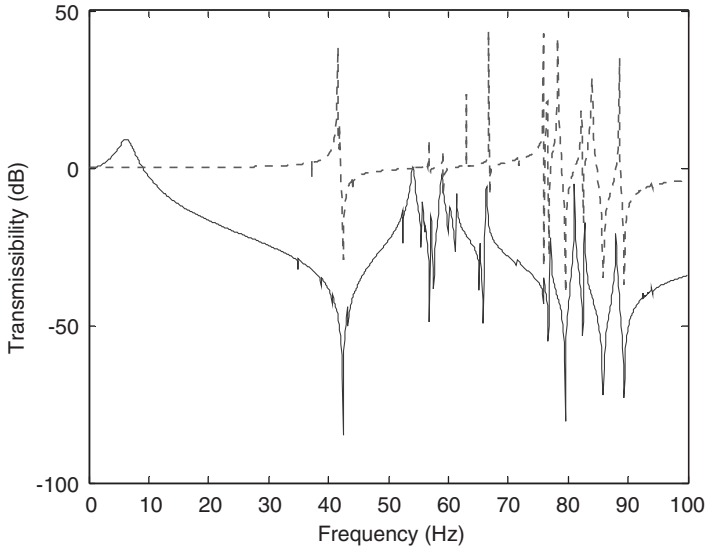

Fig. 11. The longitudinal transmissibility.

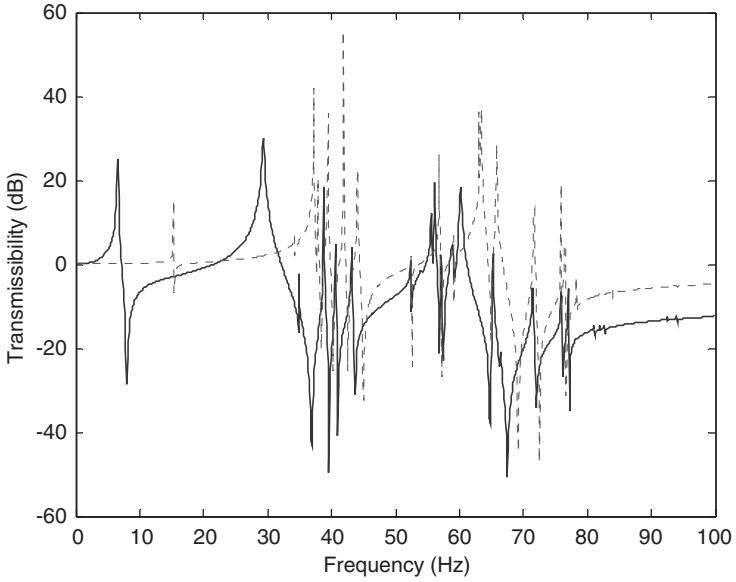

Fig. 12. The lateral transmissibility.

5. Redundancy property

The octo-strut platform is a statically indeterminate structure with redundancy. If less than or equal to two struts break, the structure will still keep the original form. Assuming the sequence numbers of the failed struts are n_1 and n_2, i.e. their stiffness is zero, the stiffness matrix of the

platform, $\mathbf{K}_{\text{fail}}$, becomes

$$\mathbf{K}_{\text{fail}} = \mathbf{K}_{\text{platform}} - k \begin{bmatrix} \sum_{i=n_1,n_2} \mathbf{u}_i \mathbf{u}_i^{\mathrm{T}} & \sum_{i=n_1,n_2} \mathbf{u}_i \mathbf{s}_i^{\mathrm{T}} \\ \sum_{i=n_1,n_2} \mathbf{s}_i \mathbf{u}_i^{\mathrm{T}} & \sum_{i=n_1,n_2} \mathbf{s}_i \mathbf{s}_i^{\mathrm{T}} \end{bmatrix}, \tag{36}$$

which is still a full rank matrix. In Eq. (27), by substituting $\mathbf{K}_{\text{fail}}$ for $\mathbf{K}_{\text{platform}}$, the nature frequencies of the isolation system with failure can be computed, which are listed in Table 2. When the mount stiffness of one or two struts is decreased as a result of failure, changes caused in the nature frequencies are small. The lateral displacements at the top of the satellite with one and two failed struts are 0.0297 and 0.0299 m, respectively. The system is still in the safe region. Fig. 13 shows transmissibility of longitudinal acceleration with one or two failed struts. Comparing with that of normal condition, their deviation is also sufficiently small.

Table 2
The nature frequencies (Hz) of the vibration isolation system with failures

Type of failures	1st	2nd	3rd	4th	5th	6th
Normal condition	6.500	8.521	8.922	8.901	67.86	68.47
One mount stiffness	5.920	8.056	8.899	8.909	67.58	68.46
Two mount stiffness	5.602	7.355	8.866	8.900	67.31	68.44

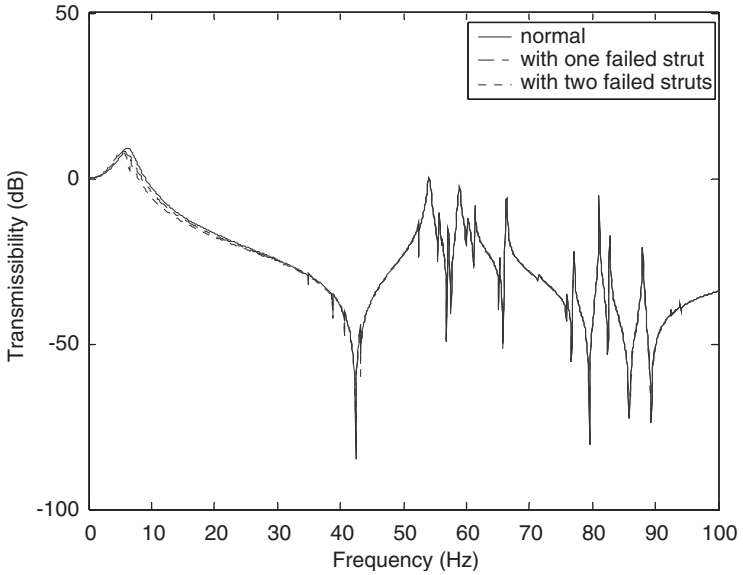

Fig. 13. The longitudinal transmissibility with one or two failed struts.

6. Conclusion

In the present paper, an octo-strut vibration isolation platform is developed. An application of this platform is the whole-spacecraft vibration isolation. From the aspect of reliability, an important advantage of this type of structure is the redundancy provided by its statically indeterminate structure. If any strut has failure, the structure will still keep the original form and a disaster can be avoided.

To avoid the possibility that the spacecraft interacts with the fairing, a coupling stiffness method is proposed for reinforcing the rotation stiffness. Analytical study shows that it can increase the rotation stiffness effectively without any influence on the longitudinal stiffness.

References

[1] Z.J. Geng, L.S. Haynes, Six degree-of-freedom active vibration control using the Stewart platforms, *IEEE Transactions on Control Systems Technology* 2 (1) (1994) 45–53.

[2] J. Spanos, Z. Rahman, G. Blackwood, A soft 6-axis active vibration isolation, in: *Proceedings of the American Control Conference*, Seattle, Washington, June 1995, pp. 412–416.

[3] B. Dasgupta, T.S. Mruthyunjaya, Closed-form dynamic equations of the general Stewart platform through the Newton–Euler approach, *Mechanism & Machine Theory* 33 (7) (1998) 993–1012.

[4] Z. Ji, Study of the effect of leg inertia in Stewart platforms, in: *IEEE International Conference on Robotics and Automation*, Atlanta, 1993, pp. 121–126.

[5] J.E. McInroy, J.C. Hamann, Design and control of flexure jointed hexapods, *IEEE Transactions on Robotics and Automation* 16 (4) (2000) 372–381.

[6] J.E. McInroy, Modeling and design of flexure jointed Stewart platforms for control purposes, *IEEE/ASME Transactions on Mechatronics* 7 (1) (2002) 95–99.

[7] J.E. McInroy, Dynamic modeling of flexure jointed hexapods for control purpose, in: *IEEE International Conference on Control Applications*, August 1999, pp. 508–513.

[8] J.E. McInroy, G.W. Neat, J.F. O'Brien, A robotic approach to fault-tolerant, precision pointing, *IEEE Robotics & Automation Magazine* 6 (4) (1999) 24–31, 37.

[9] D.C. Johnson, S.P. Wilke, R.K. Darling, Multi-axis whole-spacecraft vibration isolation for small launch vehicles, *SPIE Conference*, Newport Beach, CA, SPIE, Vol. 4331, 2001, pp. 153–161.

[10] D.C. Johnson, S.P. Wilke, J.P. Grosserode, Whole-spacecraft vibration isolation system for the GFO/Taurus mission, *SPIE Conference on Passive Damping and Isolation*, Newport Beach, CA, USA, SPIE, Vol. 3672, 1999.

[11] K.K. Denoyer, C. Johnson, Recent achievements in vibration isolation systems for space launch and on-orbit application, *52nd International Astronautical Congress*, Toulouse, France, 2001.

[12] D.L. Edberg, C.D. Johnson, On the development of a launch vibration isolation system, *SPIE Conference*, San Diego, CA, SPIE, Vol. 3045, 1997, pp. 31–37.

[13] T.T. Hyde, L.P. Davis, Optimization of multi-axis passive isolation systems, *SPIE Conference*, San Diego, CA, SPIE, Vol. 3327, 1998, pp. 399–410.